

Article

Investigating the Impact of Green Space Ratio and Layout on Bioaerosol Concentrations in Urban High-Density Areas: A Simulation Study in Beijing, China

Wenchen Jian, Hao He, Boya Wang and Zhicheng Liu *

School of Landscape Architecture, Beijing Forestry University, Beijing 100083, China; jianwenchen@bjfu.edu.cn (W.J.); siiiigma@foxmail.com (H.H.); boyawang@bjfu.edu.cn (B.W.)

* Correspondence: zhicheng_liu@bjfu.edu.cn

Abstract: The COVID-19 pandemic significantly impacted global development. Through bioaerosols emitted by human respiration, respiratory infectious diseases, including COVID-19, are transmitted. The bioaerosol concentrations can be affected by the urban climate and morphology. However, the effects of urban green spaces on bioaerosol concentrations remain unclear. Focusing on the dormitory area of Beijing Forestry University, this study first investigated the influence of different green space ratios on the average bioaerosol concentrations using the ENVI-met software. Moreover, both overall and local green space layouts were analyzed for their impact on bioaerosol concentrations. The results indicated that ventilation conditions were the primary factor influencing bioaerosol concentrations. During peak congestion, a 10% increase in the green space ratio resulted in a 2% rise in the average bioaerosol concentration. Furthermore, a distributed layout resulted in a 1.3% higher average bioaerosol concentration than a concentrated layout with an equivalent green space ratio. Enacting strategies such as Roadside Green Spaces Retreat, Road Spaces Expansion, and Intersection Green Spaces Chamfering led to reductions in local bioaerosol concentrations by up to 17.7%, 18.44%, and 12.69%, respectively. This study highlights the importance of adjusting green space layouts in urban high-density areas after the pandemic, reducing the risk of population exposure to bioaerosol concentrations.



Citation: Jian, W.; He, H.; Wang, B.; Liu, Z. Investigating the Impact of Green Space Ratio and Layout on Bioaerosol Concentrations in Urban High-Density Areas: A Simulation Study in Beijing, China. *Sustainability* **2024**, *16*, 3688. <https://doi.org/10.3390/su16093688>

Academic Editor: Saif Uddin

Received: 20 March 2024

Revised: 18 April 2024

Accepted: 18 April 2024

Published: 28 April 2024



Copyright: © 2024 by the authors. Licensee MDPI, Basel, Switzerland. This article is an open access article distributed under the terms and conditions of the Creative Commons Attribution (CC BY) license (<https://creativecommons.org/licenses/by/4.0/>).

Keywords: respiratory infections; bioaerosol concentrations; urban high-density areas; green space ratio; green space layout; ENVI-met

1. Introduction

The global spread of the COVID-19 pandemic has significantly impeded the development of nations worldwide. Several respiratory infectious diseases, including COVID-19, can be transmitted through airborne bioaerosols. Bioaerosols are gaseous-dispersed systems comprising solid or liquid particles within a gaseous medium [1]. Bioaerosols containing microbial organisms or biologically active molecules are referred to as bioaerosols [2]. Bioaerosol particles with small diameters ($\leq 5 \mu\text{m}$) potentially lead to higher viral loads and larger concentrations than larger particles, primarily coming from human respiratory activity [3]. These smaller droplets can remain suspended in the air for extended periods, forming bioaerosols, and can be transported over considerable distances [4]. Notably, a previous study found detectable levels of COVID-19 in bioaerosols three hours after nebulization [5], underscoring the significant risk posed by these bioaerosol droplets in spreading infectious diseases, including several respiratory infectious diseases such as COVID-19.

With the ongoing global urbanization trend, nearly two-thirds of the world's population will reside in cities by 2050 [6]. Epidemics swiftly spread in densely populated large cities due to a high population density and mobility, posing challenges to prevention and control measures. In the post-epidemic era, acknowledging the reality of long-term

coexistence with viruses and reducing the concentration of bioaerosols in urban air is paramount for urban disease prevention and control and as well as the overall health of urban residents [7–9].

In the post-pandemic era, there is a growing emphasis on urban health and safety. Disease transmission within cities is a multifaceted interplay between urban climatic factors and urban morphology. Urban climatic factors, particularly ventilation status, significantly influence disease transmission dynamics [10]. Low wind speeds, leading to heightened concentrations of air pollutants, can prolong the presence of viruses within pollutants, elevating the risk of disease transmission [11,12]. Additionally, the mortality rate among infected individuals closely correlates with the accumulation of air pollutants resulting from inadequate air circulation in urban areas. Prolonged exposure to PM_{2.5} is associated with a notable rise in COVID-19 mortality [13]. Urban morphology, on the other hand, predominantly affects disease transmission by affecting urban ventilation conditions. Building morphology and layouts substantially influence local urban ventilation conditions [14]. During low wind speeds, the risk of infection in building courtyards equals that of indoor spaces. Properly designed courtyard areas can effectively mitigate this risk [15]. Building density, public transportation, and urban sanitation can exacerbate disease transmission risks [16]. At the community level, alterations in city morphology can enhance ventilation, facilitating pollutant dispersion and reducing pollutant concentrations, thereby minimizing infection risks [17].

As integral components of urban infrastructure, urban green spaces enhance urban health and safety [18,19]. The historical practice of constructing urban parks in the 18th century in the UK, aimed at improving urban hygiene and controlling disease spread, is a testament to their importance. The rampant infectious diseases of the 19th century prompted proactive urban environment management to address public health challenges. Recent studies have indicated that urban green spaces play a crucial role in mitigating air pollutant concentrations within cities [20–24]. Plants can absorb gaseous pollutants through leaf stomata or surfaces [20,25], and they can also trap airborne particulate matter on leaves and stems [26–30]. In densely populated urban areas, well-designed green spaces with diverse plant species effectively combat air pollution [31]. Within street canyons, green spaces along roadways act as barriers, limiting the spread of pollutants such as PM_{2.5}, PM₁₀, and nitrogen dioxide emitted by vehicles, thus reducing pollutant concentrations on sidewalks and adjacent neighborhoods [32,33]. However, these green spaces may also diminish wind speeds in street canyons, reducing air circulation above rooftops and within the canyons and exacerbating pollutant accumulation [34–38]. Furthermore, urban green spaces' size, shape, and layout significantly influence particulate pollutants [39,40]. Notably, a negative correlation exists between the area of green space and PM_{2.5} levels [41]. For urban green spaces within a 2 km radius, the total edge length has a more substantial impact on PM_{2.5} than the green coverage area, which holds more significant influence within 3–5 km scales [42]. Additionally, enhancing the likelihood of green space interaction with the air, achieved through intricate shapes, reduces urban PM_{2.5} concentrations in extensive green space patches [43]. On the landscape level, a more uniform and decentralized distribution of green spaces is advantageous in curbing particulate matter emissions [44]. Furthermore, urban green spaces play a pivotal role in disease transmission dynamics. Plant leaves serve as adsorbents for bioaerosol droplets, and certain plants release chemicals that neutralize pathogens within these droplets. Research by Zhao indicates that within specific parameters, augmenting vertical greening coverage on buildings significantly lowers bioaerosol concentrations in urban environments [45].

However, the specific impact of green space ratios and layouts on bioaerosol concentrations in neighborhood-scale urban green spaces within high-density built-up areas is still under investigation. The goal of this study is to first investigate the correlation between green space ratios and bioaerosol concentrations in high-density built-up areas. Subsequently, it explores the effects of varying green space layouts on bioaerosol concentrations under consistent green space ratios. The primary task is to preliminarily simulate the im-

pect of different green space ratios and typical layout patterns on bioaerosol concentrations, laying the foundation for more in-depth, comprehensive research in the future. These examinations seek to establish a theoretical foundation for constructing green spaces in urban high-density built-up areas in the post-pandemic era.

2. Materials and Methods

In this study, we selected the dormitory area of Beijing Forestry University as our research site, with major roads serving as the source of bioaerosol pollution. Through field surveys, we obtained pedestrian flow data on these roads to calculate the bioaerosol release rates. Finally, we utilized Envi-met software to simulate bioaerosol concentrations under different green space ratios and layouts, followed by a comparative analysis.

2.1. ENVI-Met Software Introduction

ENVI-met is advanced simulation software widely used for analyzing urban microclimates. Differing from conventional urban climate modeling software, ENVI-met places a strong emphasis on the intricate interplay among structural surfaces, vegetation, and the atmospheric environment. Employing the standard convection–diffusion equation (Equation (1)), it conducts simulations for the diffusion of gases and particles [46]:

$$\frac{\partial \chi}{\partial t} + u \frac{\partial \chi}{\partial x} + v \frac{\partial \chi}{\partial y} + w \frac{\partial \chi}{\partial z} = \frac{\partial}{\partial x} (K_x \frac{\partial \chi}{\partial x}) + \frac{\partial}{\partial y} (K_x \frac{\partial \chi}{\partial y}) + \frac{\partial}{\partial z} (K_x \frac{\partial \chi}{\partial z}) + Q_x(x, y, z) + S_x(x, y, z) \quad (1)$$

where χ represents the component of a gas or particle in the atmosphere as simulated; Q_x and S_x denote the pollution source and deposition type, respectively. The pollution sources (Q_x) are classified into four categories: point sources, line sources, area sources, and volume sources. Deposition types (S_x) encompass particles deposited from the top layer, particles subject to gravity deposition, and the total loss of particles caused by deposition on leaf surfaces. The effect of gravity on pollutants, the effect of plants on pollutants, and the microclimate are all considered in ENVI-met [46].

Previous studies have consistently demonstrated the high precision of ENVI-met in modeling urban microclimates [32,47–51]. It has found application in diverse settings, such as urban settlements, street canyons, campuses, roads, and parks [52]. This study utilized ENVI-met version 5.1.1 for simulations.

2.2. Study Site

The climate in Beijing, China, falls under the warm-temperate semi-humid continental monsoon category, characterized by an average annual temperature of 14 °C and an average annual precipitation of approximately 600 mm [53]. The study focused on Beijing Forestry University in Haidian District, Beijing, China. Beijing Forestry University encompasses an area of approximately 46.4 hectares, with a built-up green space ratio of around 42.2%. The campus accommodates nearly 20,000 students and faculty members. Because a significant portion of students reside on campus, the main roads within the dormitory area, located in the southwestern part of the campus, witness high population density during commuting hours, representing a characteristic scenario of high-density built-up areas in Beijing. Therefore, the rectangular-shaped dormitory area, measuring about 250 m in length and 140 m in width, with predominantly student dormitories, was chosen as the study site. The specific layout of the roads, buildings, green spaces, and other elements within this area formed the fundamental parameters for the ENVI-met simulation (Figure 1).

2.3. Study Date and Time

Previous studies have indicated that the spread of new coronaviruses intensifies in densely populated areas [10]. Moreover, a brief environmental exposure has been identified as a potential pathway for infection. This emphasizes the importance of bioaerosol concentrations during pedestrian peak hours in densely populated regions, which greatly influence the transmission dynamics of respiratory infectious diseases. As a result, the

study focused on weekdays between 11:00 and 13:00, coinciding with the peak pedestrian hours in the study area. Students frequently travel between dormitories and academic buildings before and after classes during this time. Field studies were conducted from Monday, 8 May 2023, to Friday, 12 May 2023, between 11:00 and 13:00 each day to capture the peak pedestrian flow in the study site.

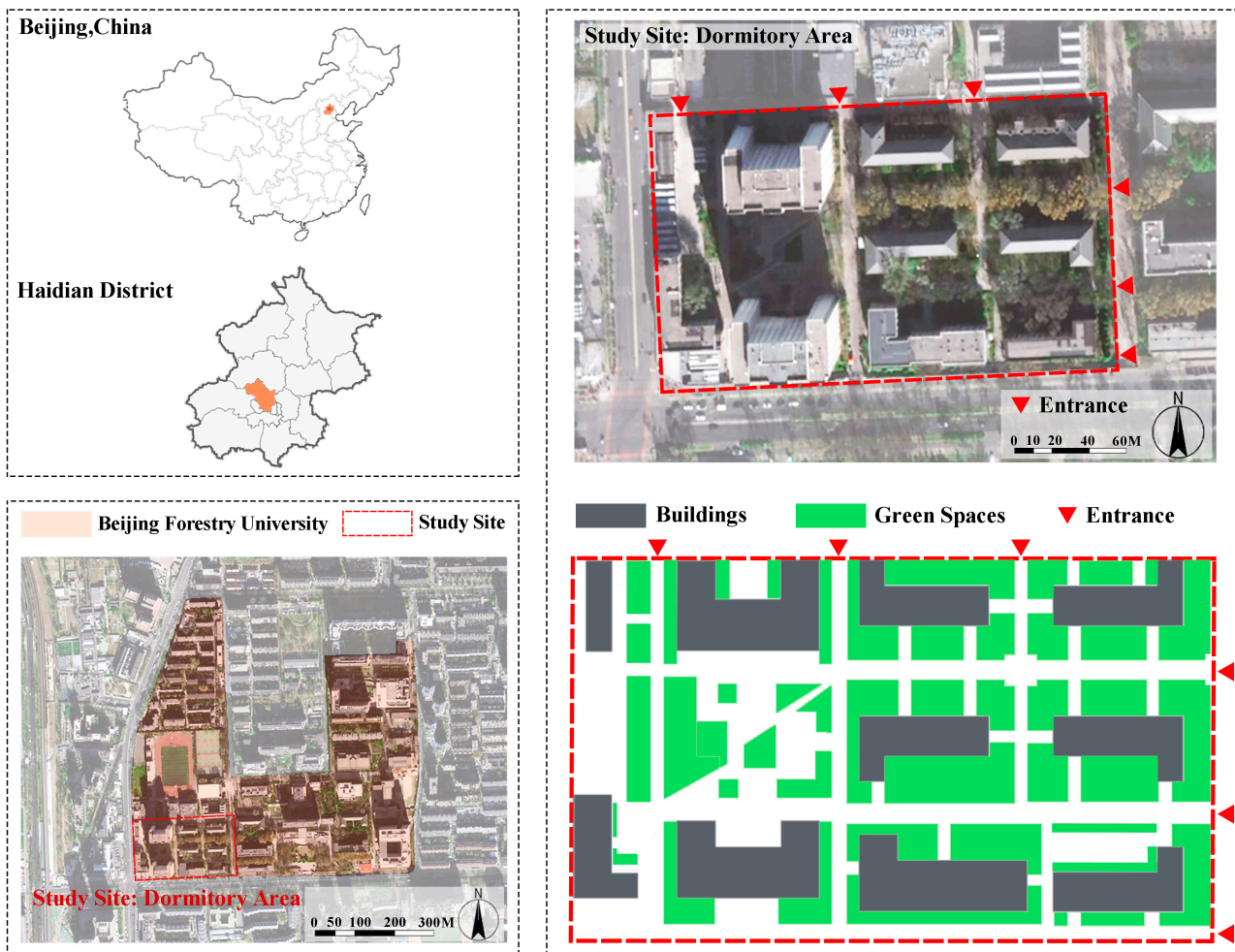


Figure 1. Study site: dormitory area in Beijing Forestry University, Haidian District, Beijing, China. Source: <http://guihuayun.com> (accessed on 10 June 2023).

2.4. Pollution Source Identification

On campuses, bioaerosols containing pathogens stem from human respiratory activities, with roads constituting the principal source of bioaerosol pollution. For simulations utilizing the ENVI-met model in this study, bioaerosols were designated as particle pollution sources [17,45]. The particles were characterized by a diameter of $5\ \mu\text{m}$ [3,4] and a density of $1 \times 10^3\ \text{kg}/\text{m}^3$ [54]. The bioaerosol concentration experiences notable variations at the campus scale due to the combined influence of background concentration and foot traffic. Therefore, the software's source model was configured to include background pollutants and linear-traffic-related sources in this study. The background concentration was $0.1\ \mu\text{g}/\text{m}^3$ [45]. The production rate of the linear source depended on both the pedestrian flow on the roadway and the rate of bioaerosol generation resulting from pedestrians' respiratory activities.

2.4.1. Current Roads and Pedestrian Flow Statistics

Given the substantial variations in pedestrian traffic along different roads within the study site, conducting time- and location-specific pedestrian flow counts was imperative. In this context, the current road network and pedestrian flow conditions were amalgamated, dividing the study area into 14 major road sections (Figure 2). Pedestrian flow statistics were aggregated over five days for each time slot and location, providing the foundational statistics for determining the pollution release rate of the ENVI-met-modeled pollutant sources (Table 1).

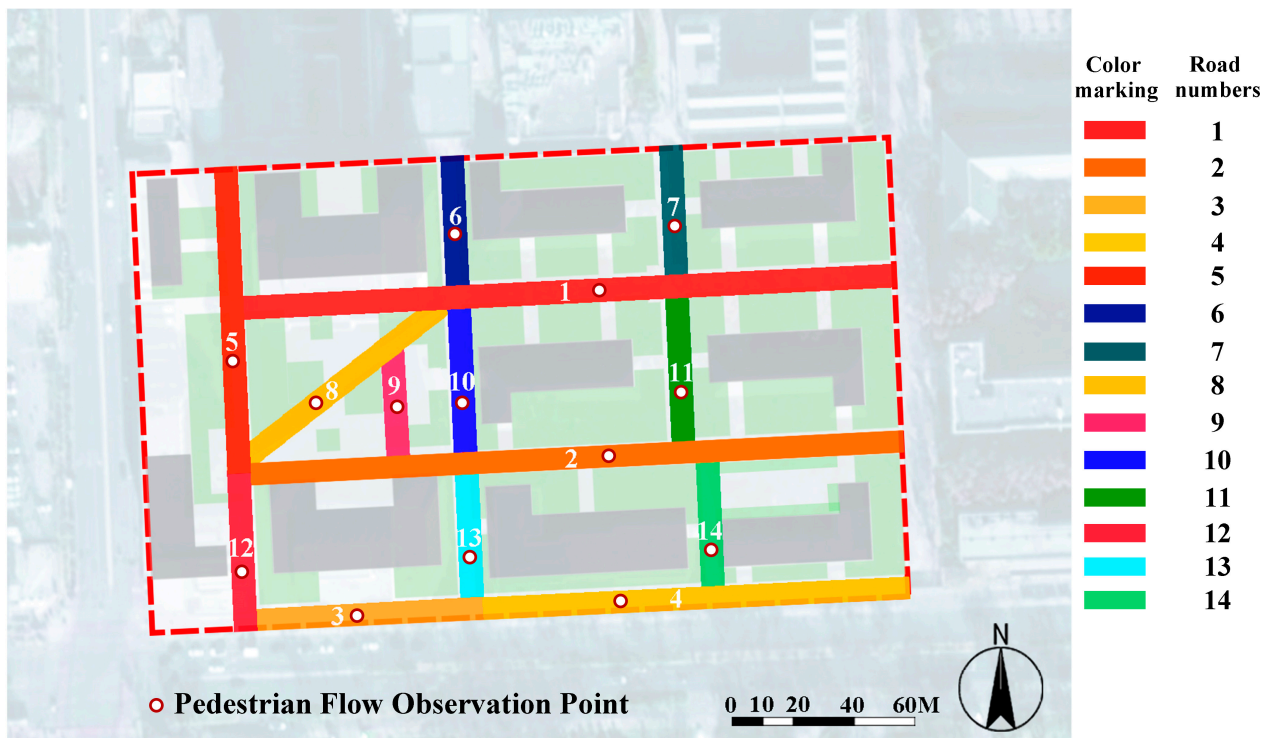


Figure 2. Major roads and their numbers in the study site.

Table 1. Pedestrian flow on major roads during 11:00–11:59 AM and 12:00–12:59 AM, from 8 May–12 May 2023.

Road Numbers	Road Pedestrian Flow (People/min) 11:00–11:59 AM						Road Pedestrian Flow (People/min) 12:00–12:59 AM					
	5.5	5.8	5.9	5.10	5.11	5-Day Average	5.5	5.8	5.9	5.10	5.11	5-Day Average
1	14	17	17	12	13	15	13	9	6	13	16	11
2	6	11	22	9	7	11	10	9	10	11	12	10
3	13	10	9	9	13	11	12	9	10	14	10	11
4	2	1	2	1	2	2	1	2	1	4	2	2
5	3	3	3	3	4	3	3	3	6	3	2	3
6	16	34	24	21	29	25	22	17	25	21	16	20
7	12	7	10	8	10	9	10	7	4	7	12	8
8	13	16	17	13	19	16	8	11	17	14	16	13
9	9	16	13	12	20	14	11	10	14	11	13	12
10	11	13	15	11	14	13	8	9	11	10	14	10
11	9	8	10	6	5	8	9	5	5	4	8	6
12	14	9	12	9	13	11	10	9	12	12	9	10
13	6	6	9	5	4	6	5	5	7	4	10	6
14	3	2	1	3	4	3	0	1	1	2	2	1

2.4.2. Calculation of Bioaerosol Release Rates

Research indicates that an adult can expel nearly 2 million droplets when sneezing, comparable to those produced during conversations [55]. A single cough can also generate about 1 million droplets [56]. Nasal and oral breathing produces approximately 1/20 and 1/3 as many droplets (with a diameter $>1 \mu\text{m}$) as coughing, respectively [55]. This study considered a compromise of 1/10, assuming a droplet diameter of $5 \mu\text{m}$ [3,4]. Then, the mass of individual bioaerosol particles (Equation (2)) and the total mass of bioaerosols produced by a single breath from an adult was calculated (Equation (3)). Adults typically walk at a speed of about 1.5 m/s and breathe at a rate of 12–20 breaths/min. During the study period, pedestrians were observed to walk faster; thus, the upper limit of 20 breaths/min was used. Within a 3 s timeframe of a single breath, pedestrians cover a distance of 4.5 m (Equation (4)). It was approximated that the bioaerosols produced by a single breath were uniformly distributed over this distance. Consequently, an adult's bioaerosol pollution release rate was calculated to be $0.485 \mu\text{g}/\text{m}\cdot\text{s}\cdot\text{person}$ (Equation (5)). The study calculated the bioaerosols' linear source pollution release rate by utilizing the average pedestrian flow data for each roadway during each time slot (Equation (6)) (Table 2).

$$m = \rho \times \frac{4}{3} \pi r^3 \quad (2)$$

$$M = n \times m \times k \quad (3)$$

$$l = v \times t \quad (4)$$

$$V_0 = \frac{M}{l \times t} \quad (5)$$

$$V = V_0 \times \frac{N}{60} \quad (6)$$

Table 2. Bioaerosol release rates for linear pollutant sources on major roads during 11:00–11:59 AM and 12:00–12:59 AM.

Road Numbers	Bioaerosol Release Rate for Linear Pollutant Source, 11:00–11:59 AM ($\mu\text{g}/\text{m}\cdot\text{s}$)	Bioaerosol Release Rate for Linear Pollutant Source, 12:00–12:59 AM ($\mu\text{g}/\text{m}\cdot\text{s}$)
1	0.118	0.092
2	0.089	0.084
3	0.087	0.089
4	0.013	0.016
5	0.026	0.027
6	0.200	0.163
7	0.076	0.065
8	0.126	0.107
9	0.113	0.095
10	0.103	0.084
11	0.061	0.050
12	0.092	0.084
13	0.049	0.050
14	0.021	0.010

2.5. Simulation Plan Development

2.5.1. Configuration of ENVI-Met Main Parameters

The fundamental model of ENVI-met adopts a grid structure encompassing the x -axis, y -axis, and z -axis. Considering the scale of the study area, a grid measuring $50 \times 50 \times 40$ was employed, with each grid unit measuring $5 \text{ m} \times 5 \text{ m} \times 4 \text{ m}$. Since pedestrians are only exposed to high concentrations of bioaerosols containing viruses for a brief duration sufficient to cause infection, the simulation was concentrated on the two-hour period from 11:00 to 13:00 on 10 May 2023, when the pedestrian flow reaches its peak

during the day. Other vital parameters were configured based on relevant meteorological data from Haidian District, Beijing (Table 3).

Table 3. Main parameter settings for ENVI-met.

Parameter Category	Parameter Name	Input Value
Geographic location	Latitude and longitude	Beijing, China (39.96° N, 116.30° E)
Time zone	Time zone	China Standard Time/GMT + 8
Simulation time	Start time	10 May 2023, 11:00 AM
	End time	10 May 2023, 1:00 PM
	Duration	2 h
Meteorological conditions (Source: The real-time data from http://hz.hjhj-e.com/ , accessed on 15 May 2023)	Wind direction (0:N, 90:E, 180:S, 270:W)	135
	Wind speed	2 m/s
	Initial temperature	24 °C
	Relative humidity	24%
Plant parameters	Grass	25 mm height, 2D grass
	Trees	10 m height, 2D trees
Pollution source settings	Pollution source type	Linear (line)
	Pollution source category	Particle
	Background pollution concentration	0.1 µg/m ³
	Linear pollutant source release rate	Refer to Table 2

2.5.2. Model Construction: Impact of Green Space Ratios on Bioaerosol Concentrations

The current green space ratio in the study area is approximately 36%, while the ratio of existing buildings and main roads totals about 53%. Consequently, the green space ratio can be increased to approximately 47%. While preserving the existing building and main road configurations, all green areas were transformed into a plantation pattern comprising trees + grass. The woodland closeness was maintained at nearly 100% (Figure 3). To explore the influence of green area ratio on bioaerosol concentration and wind speed, six models were constructed with green area ratios of 0%, 10%, 20%, 30%, 40%, and 47% (Figure 4).

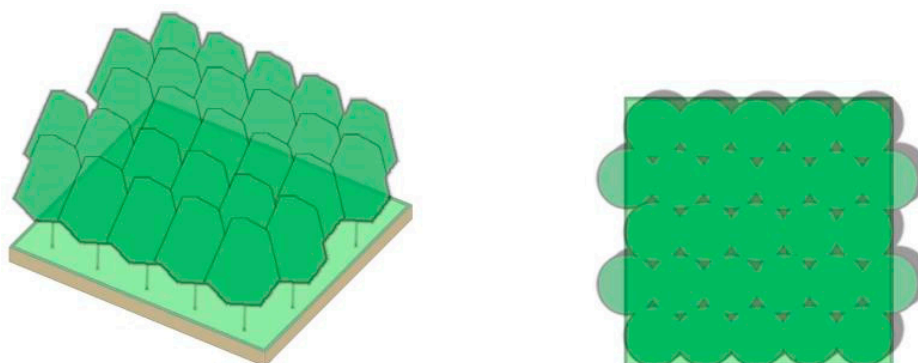


Figure 3. Plantation pattern: trees + grass.

2.5.3. Model Construction: Impact of Green Space Layouts on Bioaerosol Concentrations

In order to maintain the existing green space ratio (approximately 36%), all green areas utilized trees + grass planting patterns. Within 11:00–11:59, four groups of 17 models were constructed to explore the effect of overall and local green space layouts on bioaerosol concentrations.

For the overall layout, models in Group 1 explored the impact of distributed and concentrated green space layouts on the average bioaerosol concentrations. For the local layout, the influence of green space arrangements on bioaerosol concentrations was investigated at specific locations, such as busy roads and intersections, where the pollutant release rate was high. Models in Group 2 and Group 3 explored the influence of the green space layout

on bioaerosol concentrations along roads. Furthermore, the models in Group 4 explored the impact of the green space layout on bioaerosol concentrations at intersections.

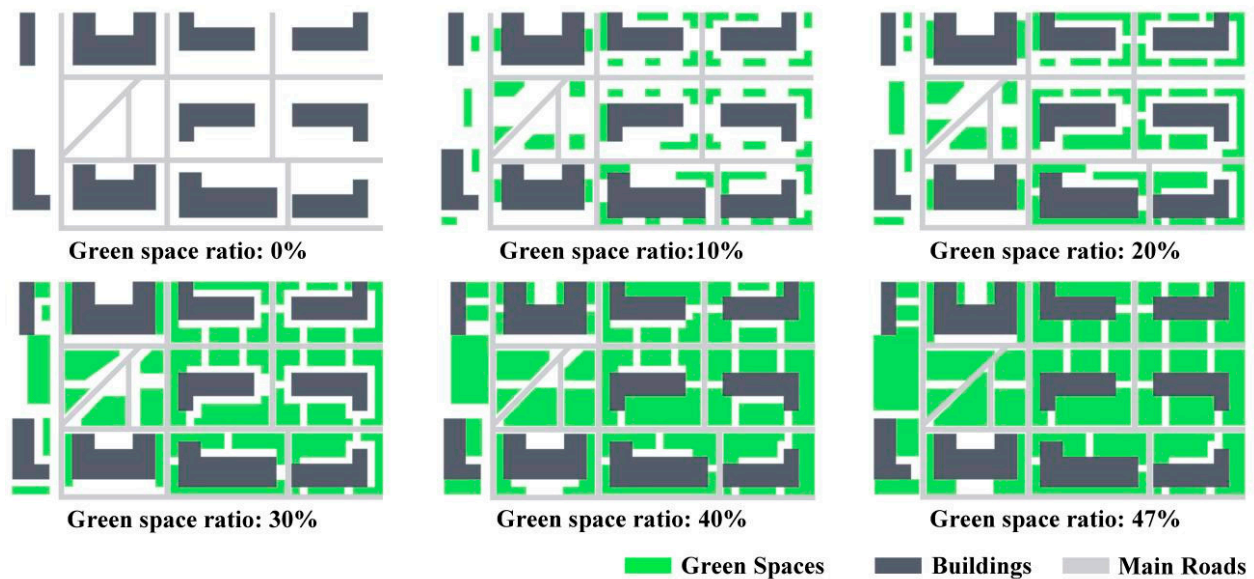


Figure 4. Simulation plan for investigating the impact of green space ratio on bioaerosol concentrations.

Overall Layouts

- Group 1: Distributed and Concentrated Layouts

In Group 1, four models were developed. Layouts 1 and 2 employed distributed layouts, distributing green spaces evenly across the study area. Layouts 3 and 4, on the other hand, adopted concentrated layouts, positioning green spaces more centrally. Specifically, Layouts 1 to 3 arranged green spaces in the west open space, while Layout 4 preserved the west open space to the maximum extent possible (Figure 5). Fragstats v4.2 software was employed to calculate two landscape pattern indices, the Number of Patches and the Split Index, for the four models. Both indices respond to the degree of green space dispersion under consistent green space area conditions, with higher values indicating more excellent dispersion [57]. The results revealed significant differences in the Number of Patches and the Split Index among models with distributed and concentrated layouts (Table 4), indicating marked disparities in the degree of green space layout dispersion.

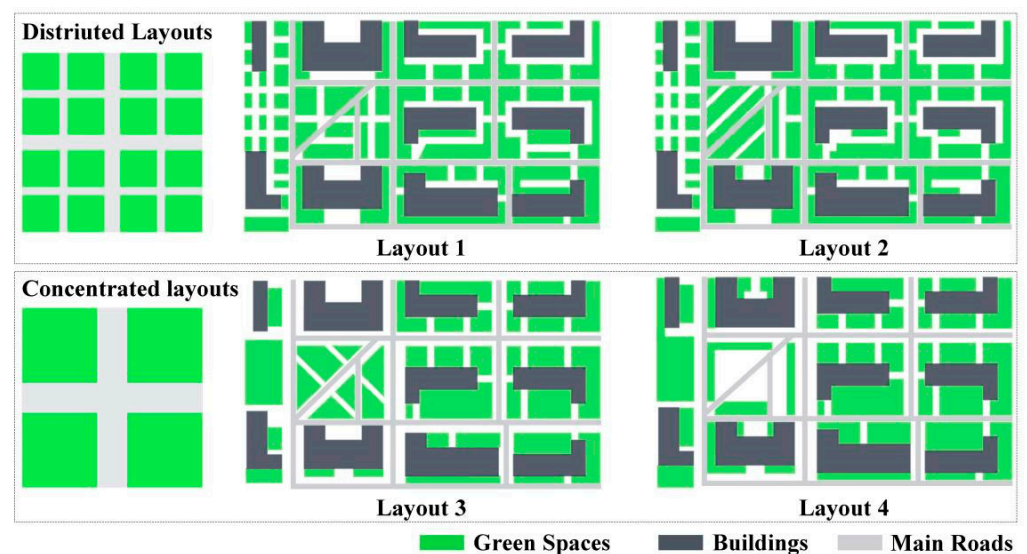


Figure 5. Group 1: Distributed and concentrated layouts.

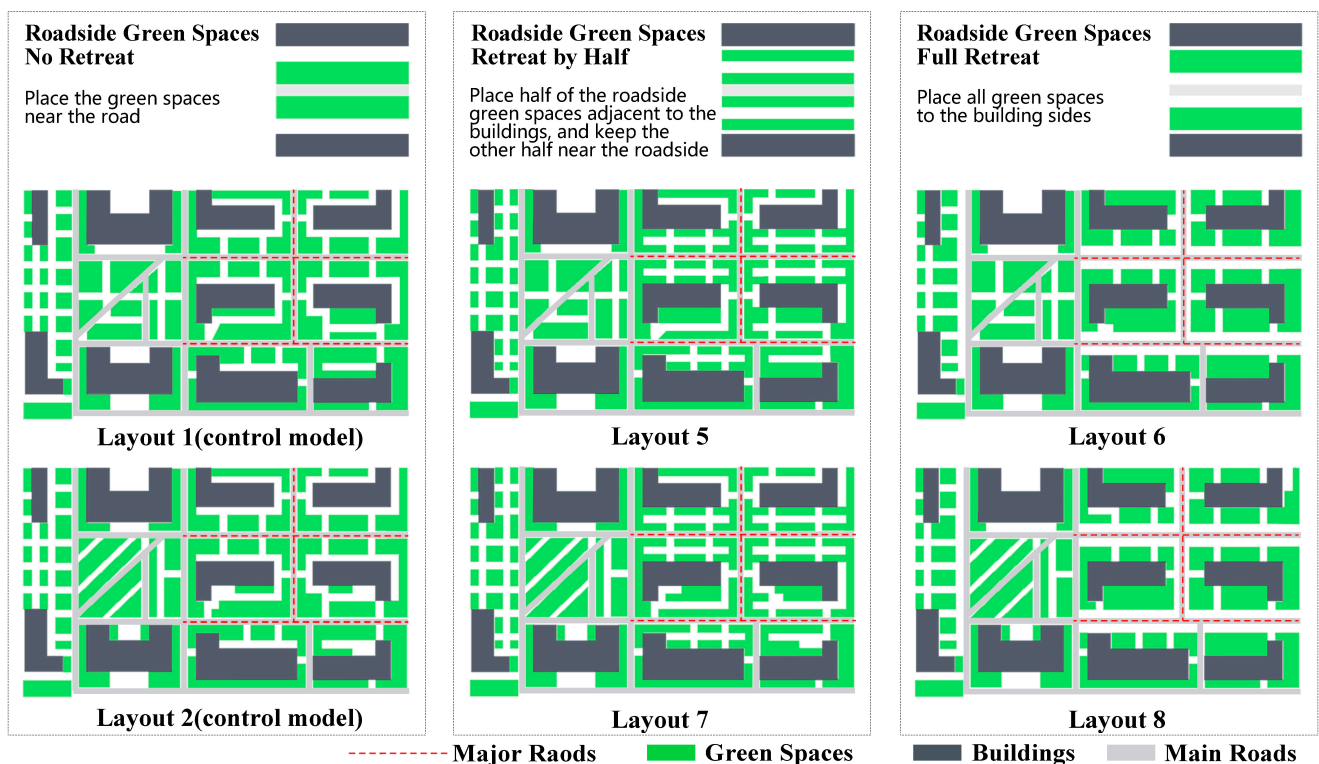
Table 4. Number of Patches and the Split Index for the layouts in Group 1.

Layouts	Number of Patches (NP)	Landscape Split Index (LSI)
Layout 1	60	42.0525
Layout 2	70	44.7683
Layout 3	38	25.1016
Layout 4	39	23.9367

Local Layouts

- Group 2: Roadside Green Spaces Retreat

In Group 2, three strategies—Roadside Green Spaces No Retreat, Roadside Green Spaces Retreat by Half, and Roadside Green Spaces Full Retreat—were employed to investigate the impact of Roadside Green Spaces Retreat on bioaerosol concentrations. Layouts 1 and 2 from Group 1 served as control models. For the green spaces on both sides of the five major roads in the east (the dashed lines in Figure 6), the control models (Layout 1 and Layout 2) maintained Roadside Green Spaces No Retreat, situating the green spaces close to the road. Layouts 5 and 7 adopted Roadside Green Spaces Retreat by Half, with half of the roadside green spaces placed near the building side and the other half retained close to the roadside. Layouts 6 and 8 utilized Roadside Green Spaces Full Retreat, situating all green spaces near the building sides (Figure 6).

**Figure 6.** Group 2: Roadside Green Spaces Retreat.

- Group 3: Road Spaces Expansion

In Group 3, three strategies—Road Space Unexpanded, Road Spaces Doubled, and Road Spaces Tripled—were employed to investigate the influence of road space width on bioaerosol concentrations. All layouts were based on Layout 3. Layout 9 maintained Road Space Unexpanded and concentrated green space on both sides of the roads, with a high pedestrian flow in the east (the dashed lines in Figure 7) serving as a control model. Subsequently, green space on both sides of the roads was gradually reduced to widen

the road space. Layout 10 adopted Road Spaces Doubled, while Layout 11 utilized Road Spaces Tripled (Figure 7). Additional green spaces were introduced to the west of the study site to maintain a consistent green space ratio.

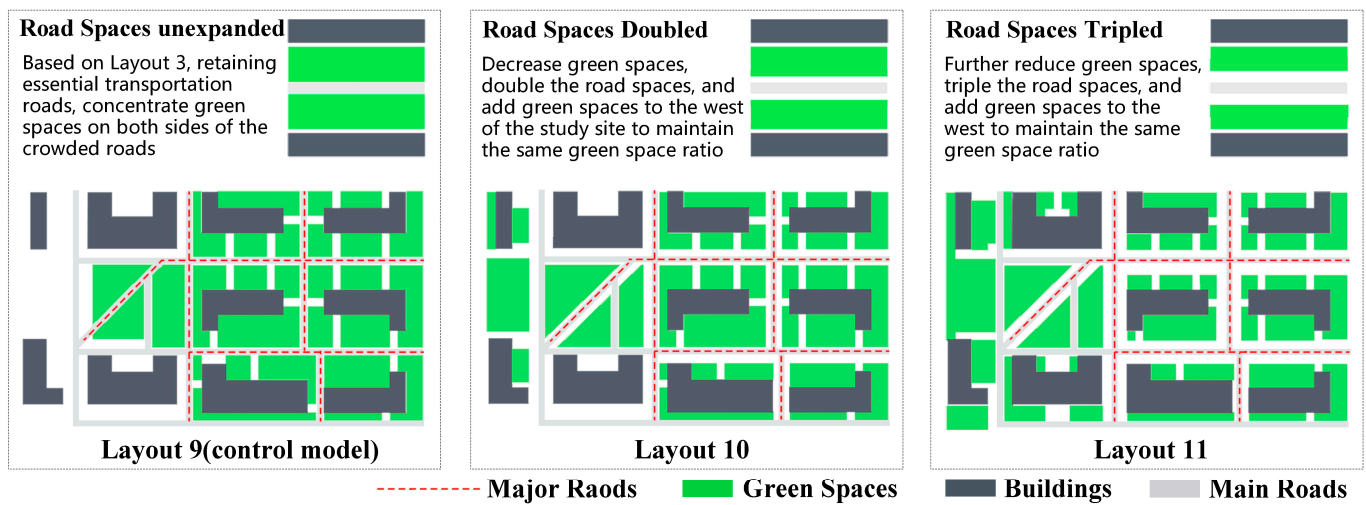


Figure 7. Group 3: Road Spaces Expansion.

- Group 4: Intersection Green Spaces Chamfering

In Group 4, four strategies—No Chamfering, Diagonal Chamfering, Quadrilateral Chamfering, and Diagonal Double Chamfering—were employed in the green spaces at the intersections to assess the effect of chamfering on bioaerosol concentrations at the intersections (the dashed box in Figure 8). Layouts 3 and 4 served as control models with No Chamfering, featuring uniformly arranged green spaces at the intersection's four corners. Subsequent models were designed to decrease green spaces at the eastern intersections, expand the intersection spaces to form a ventilated area and increase green spaces in the western location where crowds were relatively sparse, ensuring an unchanged overall green space ratio. Layouts 12 and 15 employed Diagonal Chamfering, where the wind direction (southeast wind) was considered, and chamfering was applied to the southwest and northeast corners of the green space, creating a triangular green space with a width equal to the road's width. Layouts 13 and 16 adopted Quadrilateral Chamfering for all four corners of the green space, reducing the green space by an equal amount. Layouts 14 and 17 implemented Diagonal Double Chamfering for the green space in the southwest and northeast corners only, with the area of diagonal chamfering doubled compared to Layout 12 (Figure 8).

2.6. Data Processing

Data regarding the average height of adults (approximately 1.5 m) above the ground level were extracted from the simulation results obtained through ENVI-met. The average bioaerosol concentrations and average wind speeds within the study site were computed and tabulated after excluding data from building locations and areas outside the study site.

For the simulation outcomes related to the impact of the green space ratio on bioaerosol concentrations, a Spearman correlation analysis was applied to explore the correlation of variables, considering their adherence to a normal distribution. A regression analysis was conducted for scenarios displaying significant data variations.

Regarding the simulation outcomes concerning the influence of the green space layout on bioaerosols, the results of scenarios in Group 1 were visualized as a bioaerosol concentration and wind speed distribution figure. The simulation outcomes from Groups 2, 3, and 4 were overlaid onto the differences observed in their corresponding control models to generate a relative difference in the bioaerosol concentration figure. In this representation,

the positive region indicates that the former model's data concentration is higher than the latter model's, while the negative region signifies the opposite scenario.

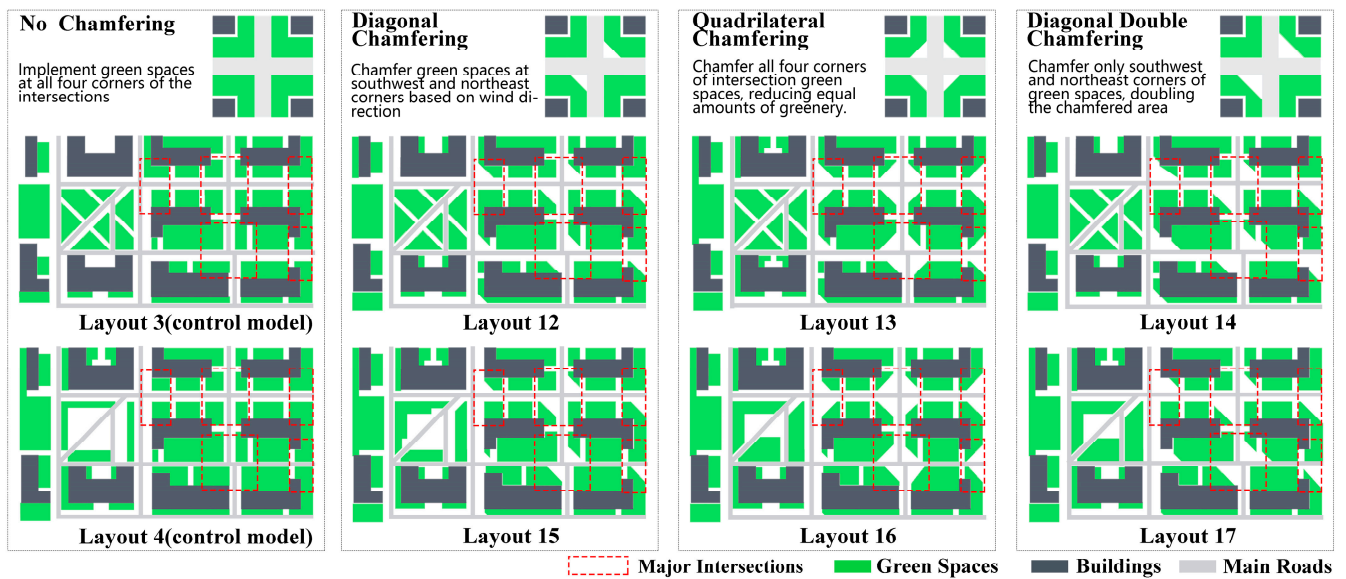


Figure 8. Group 4: Intersection Green Spaces Chamfering.

3. Results

3.1. Impact of Green Space Ratios on Bioaerosol Concentrations

Between 11:00 and 11:59, the average bioaerosol concentration and wind speed in the study area exhibited significant correlations with the green space ratio ($r = 0.994$, $p < 0.01$ and $r = -0.993$, $p < 0.01$, Table 5). With an increase in the green space ratio from 0% to 47%, the average bioaerosol concentration increased by approximately 9.6%, while the average wind speed decreased by about 53.5% (Table 6). Regression analysis revealed a 2% rise in the average bioaerosol concentration for every 10% increment in the green space ratio. Although the green space ratio had a marginal effect on reducing the average wind speed, the change remained significant until the maximum green space ratio of 47% was reached (Figure 9). The pattern of the average bioaerosol concentration with the green space ratio and wind speed in the study area persisted consistently throughout 12:00–12:59. However, the fluctuations in bioaerosol concentration were relatively subdued during the specific period of 11:00–11:59 (Figure 10).

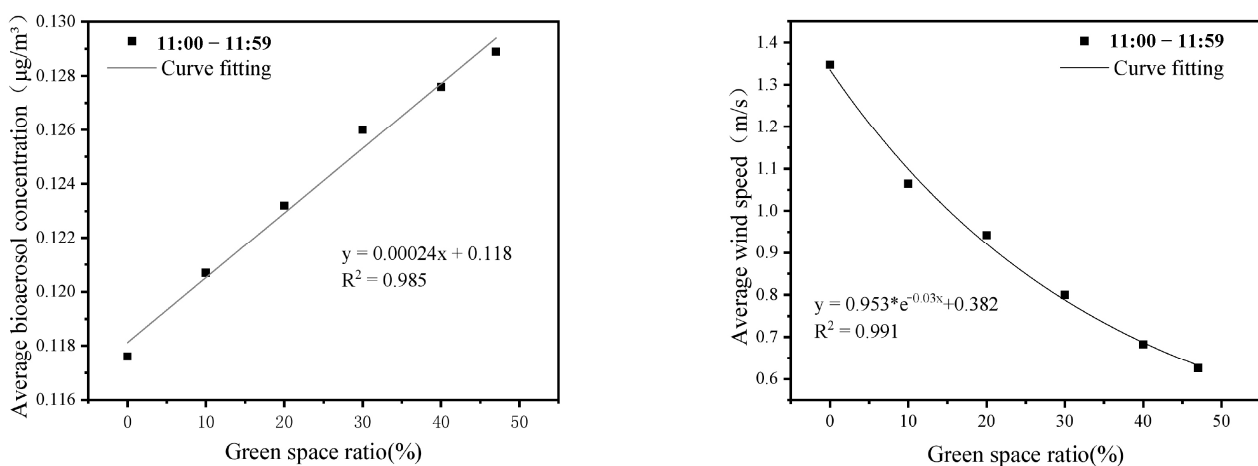


Figure 9. Regression analysis of average bioaerosol concentration and average wind speed with green space ratio in 11:00–11:59.

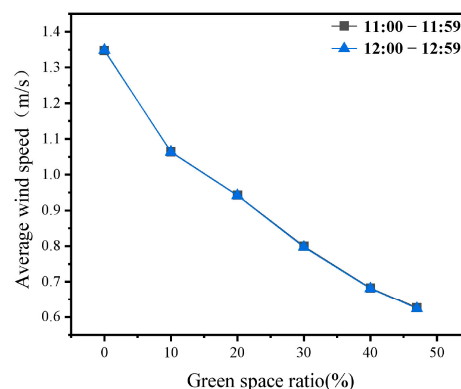
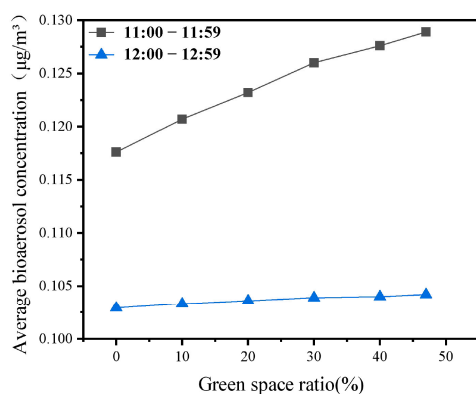
Table 5. Spearman correlation analysis.

	11:00–11:59 AM Average Bioaerosol Concentration	12:00–12:59 AM Average Bioaerosol Concentration
Green space ratio 11:00–11:59 AM	0.994 **	0.986 **
Average wind speed 12:00–12:59 AM	−0.993 **	
Average wind speed		−0.997 **

Note: ** denotes $p < 0.01$ (two-tailed), highly significant correlation.

Table 6. Average bioaerosol concentration and average wind speed at various green space ratio in different time periods.

Green Space Ratio (%)	11:00–11:59 AM Average Bioaerosol Concentration ($\mu\text{g}/\text{m}^3$)	11:00–11:59 AM Average Wind Speed (m/s)	12:00–12:59 AM Average Bioaerosol Concentration ($\mu\text{g}/\text{m}^3$)	12:00–12:59 AM Average Wind Speed (m/s)
0	0.1176	1.3474	0.1029	1.3487
10	0.1207	1.0641	0.1033	1.0632
20	0.1232	0.9425	0.1036	0.9416
30	0.1260	0.7997	0.1039	0.7973
40	0.1276	0.6824	0.1040	0.6809
47	0.1289	0.6260	0.1042	0.6234

**Figure 10.** Variations of average bioaerosol concentration and average wind speed with changing green space ratios in two time intervals.

3.2. Impact of Green Space Layouts on Bioaerosol Concentrations

3.2.1. Overall Layouts

- Group 1: Distributed and Concentrated Layouts

In Group 1, models featuring concentrated green space layouts demonstrated lower average bioaerosol concentrations and higher average wind speeds (Figure 11). The contrast between Layout 2 and Layout 4 was especially noticeable, with Layout 4 exhibiting a lower average bioaerosol concentration of approximately 1.2% and a higher average wind speed of about 15.6% compared to Layout 2 (Table 7).

Table 7. Average bioaerosol concentration and average wind speed for Group 1.

Simulation Plan Number	Average Bioaerosol Concentration ($\mu\text{g}/\text{m}^3$)	Average Wind Speed (m/s)
Layout 1	0.1271	0.7062
Layout 2	0.1272	0.6946
Layout 3	0.1256	0.8145
Layout 4	0.1256	0.8228

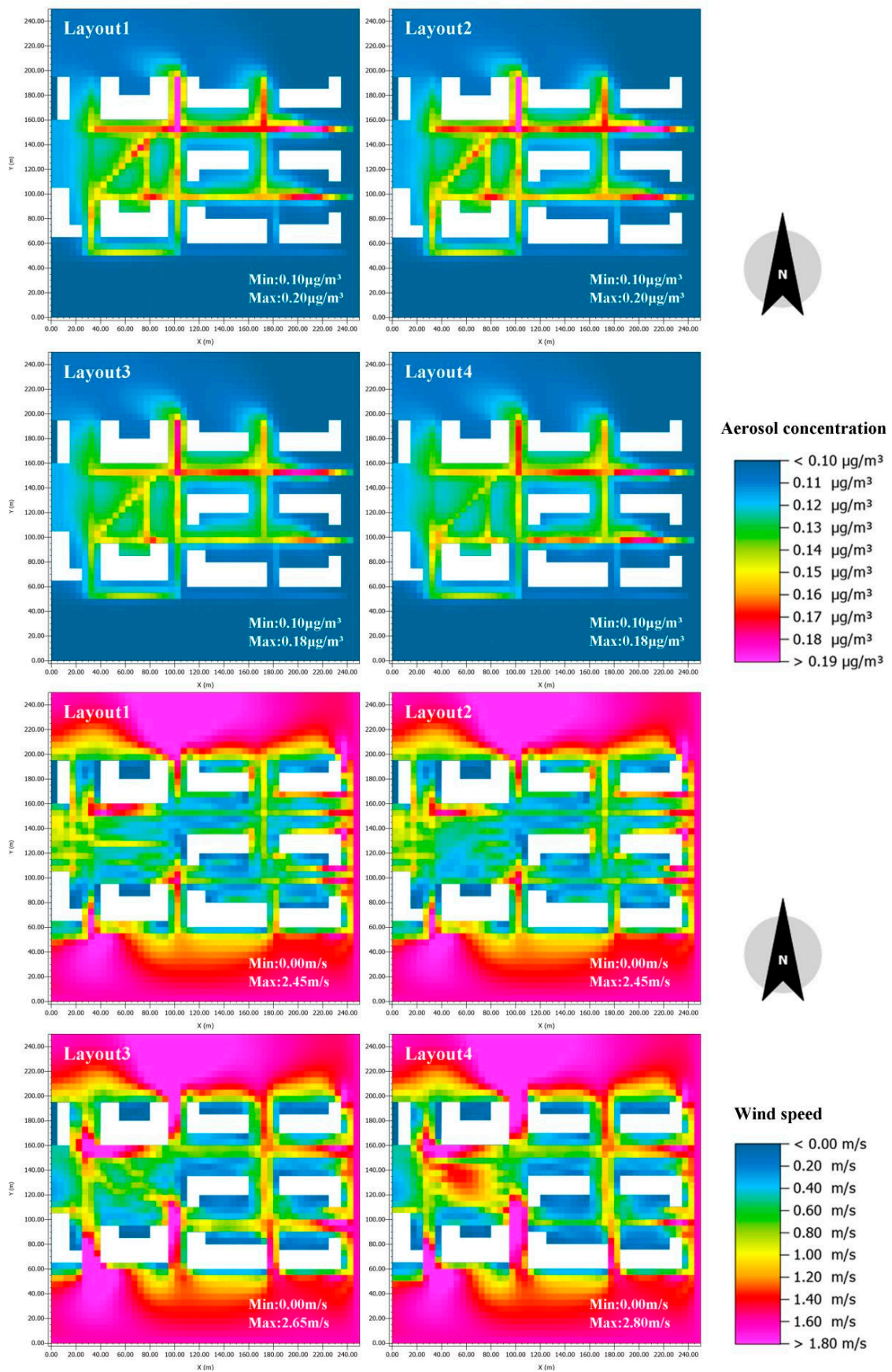


Figure 11. Average bioaerosol concentration and average wind speed distribution figure for Group 1.

3.2.2. Local Layouts

- Group 2: Roadside Green Spaces Retreat

The retreat of local green spaces led to significant decreases in bioaerosol concentrations in the adjacent road areas. However, certain regions in the west experienced a slight increase in bioaerosol concentrations. Compared to the control models (Layout 1 and Layout 2), Roadside Green Spaces Retreat by Half (Layout 5 and Layout 6) resulted in a maximum reduction of 6.8% in bioaerosol concentrations on the main eastern roads. Meanwhile, Roadside Green Spaces Full Retreat (Layout 7 and Layout 8) achieved a maximum reduction of 17.7% (Figure 12).

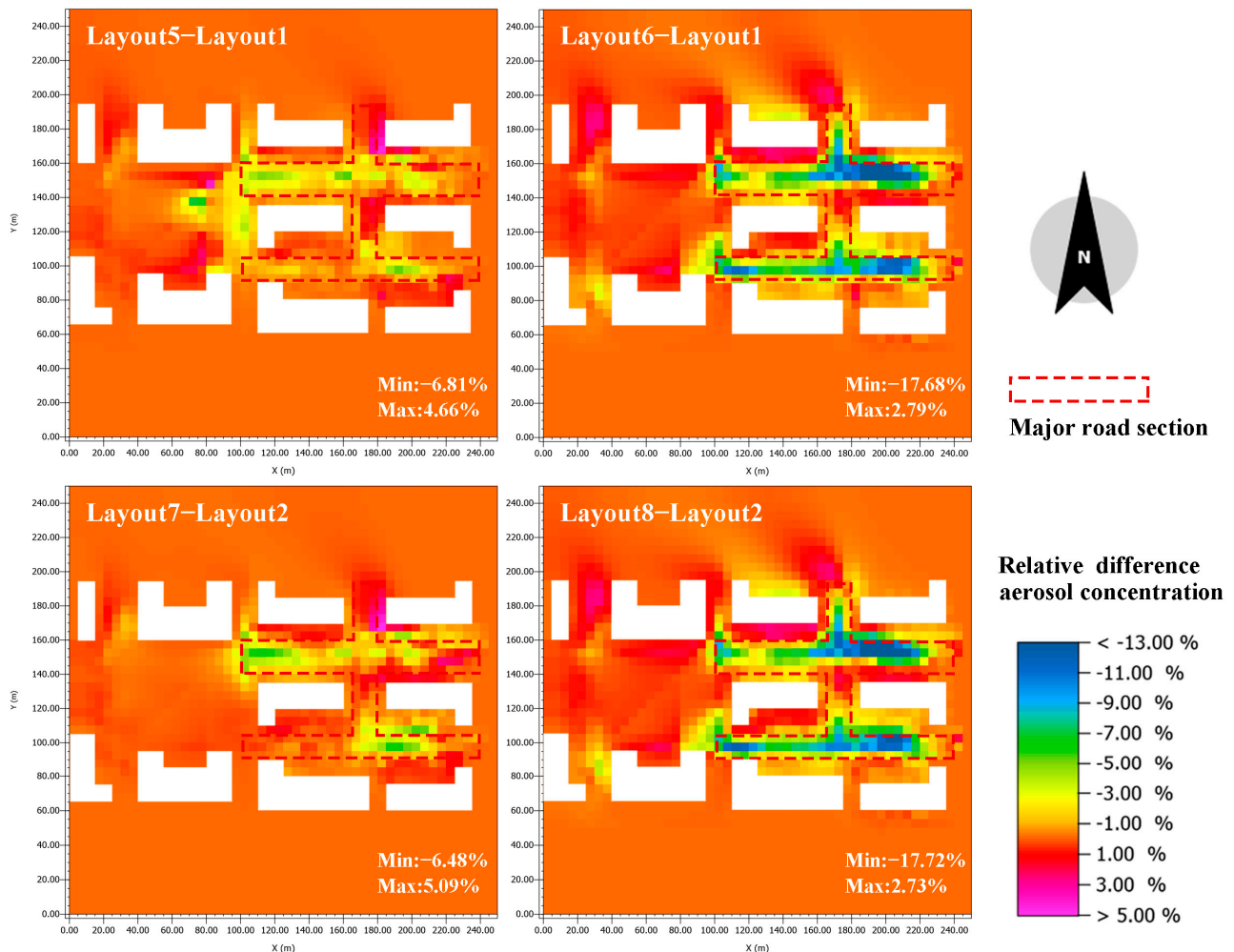


Figure 12. Relative difference bioaerosol concentration figure for Group 2.

- Group 3: Road Spaces Expansion

Road Spaces Expansion generally led to a slight decrease in the average bioaerosol concentration in the study site. Compared to the control model, Road Spaces Tripled resulted in an approximately 1.5% reduction in the average bioaerosol concentration, with negligible changes in the average wind speed (Table 8).

At local levels, areas near reduced green spaces experienced significantly lower bioaerosol concentrations, while locations with increased green spaces showed slight elevations. Compared to the control model (Layout 9), Road Spaces Doubled and Road Spaces Tripled locally reduced bioaerosol concentrations by up to 14.44% and 18.44%, respectively (Figure 13).

Table 8. Average bioaerosol concentration and average wind speed for Group 3.

Simulation Plan Number	Average Bioaerosol Concentration ($\mu\text{g}/\text{m}^3$)	Average Wind Speed (m/s)
Layout 9	0.1273	0.8283
Layout 10	0.1261	0.8391
Layout 11	0.1243	0.8314

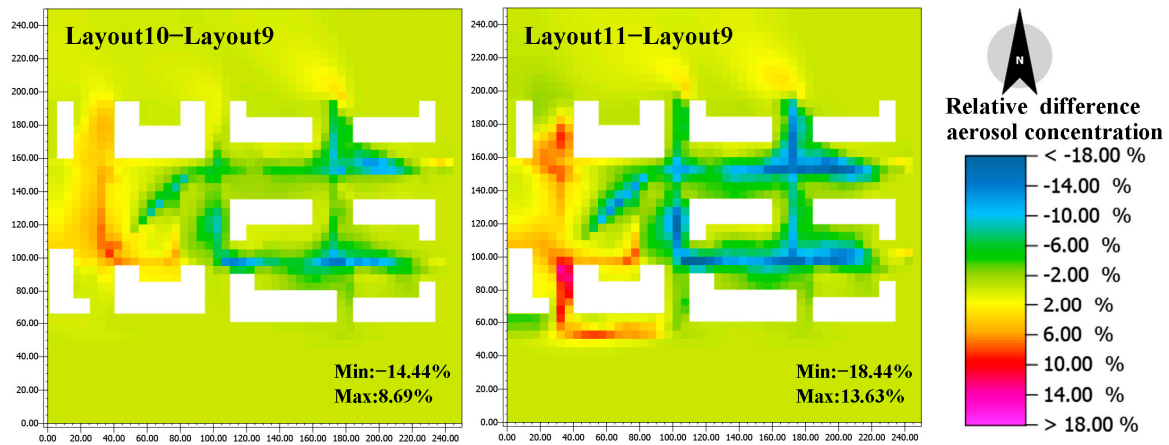


Figure 13. Relative difference bioaerosol concentration figure for Group 3.

- Group 4: Intersection Green Spaces Chamfering

Intersection Green Spaces Chamfering had a minimal impact on the overall average bioaerosol concentrations and average wind speeds at the study site. On a local scale, Diagonal Chamfering, Quadrilateral Chamfering, and Diagonal Double Chamfering exhibited maximum reductions in local bioaerosol concentrations, approximately 8.56%, 12.04%, and 12.69%, respectively, compared to the control models (Layout 3 and Layout 4). While Diagonal Chamfering and Quadrilateral Chamfering resulted in slight increases in local bioaerosol concentrations, Diagonal Double Chamfering displayed a weaker bioaerosol abatement capacity at the intersection than Quadrilateral Chamfering. Additionally, it led to bioaerosol aggregation around the intersections (Figure 14).

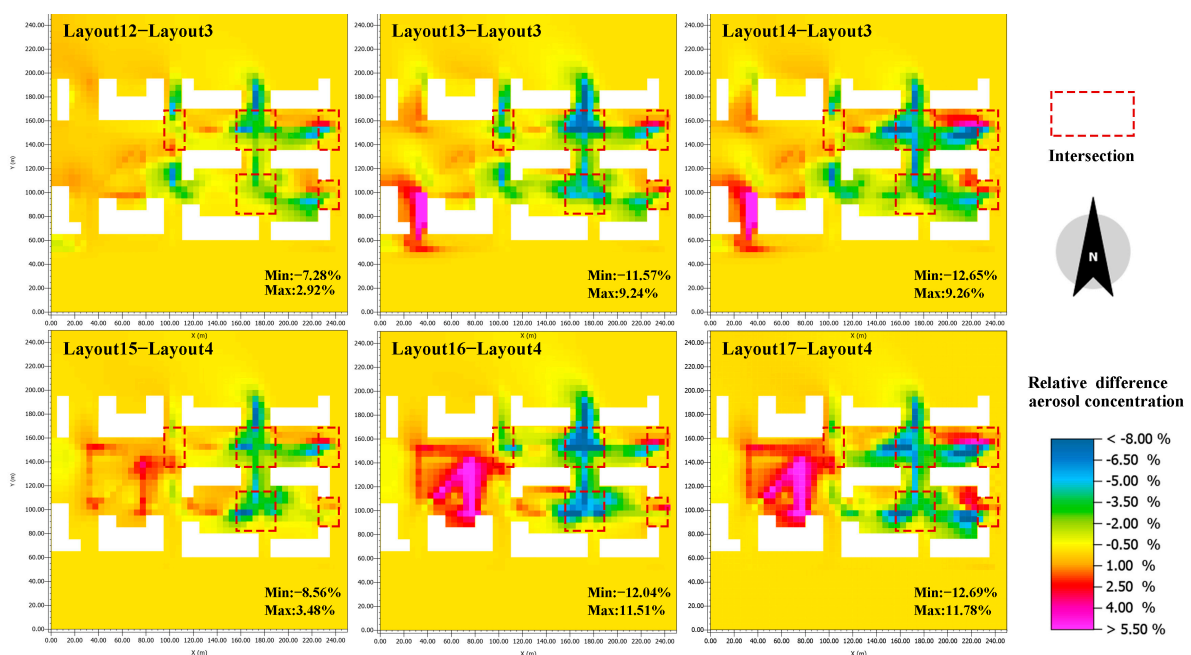


Figure 14. Relative difference bioaerosol concentration figure for group 4.

4. Discussion

1. Plants exhibited an absorptive effect on bioaerosols; however, an increase in the green space ratio resulted in a significant decrease in the average wind speed at the site and a notable increase in the average bioaerosol concentrations. In contrast, previous studies conducted on the urban scale have shown a negative correlation between the size of urban green spaces and the concentration of air pollutants. A positive correlation has been observed in their effectiveness in mitigating pollutants such as PM_{2.5} [40,41]. The difference between these findings could be attributed to the limited capacity of small-scale urban green spaces to rapidly reduce pollutant concentrations through plant absorption, especially when facing a substantial quantity of bioaerosol pollutants. During short timeframes, compromised ventilation leads to the aggregation of bioaerosols that exceeds the capacity of plant uptake of bioaerosols. On the other hand, urban green spaces serve multiple ecological functions, including climate change mitigation [58], mitigation of urban heat islands [17,59], reduction in noise pollution [17,23], and enhancement of public health [60]. Therefore, reducing the size of green spaces to control bioaerosol concentrations is not advisable. When planning urban green spaces within densely built city areas, emphasis should be placed on enhancing ventilation in densely populated areas to prevent the aggregation of bioaerosols through a rational layout while ensuring the green space scale.

2. Compared to distributed layouts, concentrated layouts exhibited a slight reduction in the average bioaerosol concentrations. According to the linear regression results of the average bioaerosol concentration concerning the green space rate at 11:00–11:59, this reduction amounted to a minimum effect equivalent to a 6.5% decrease in the green space rate, representing approximately one-sixth of the current green space scale (current green space ratio: 36%). Conversely, previous studies investigating the impact of green space layouts on air pollutants at the urban scale have suggested that a more homogeneous and decentralized distribution of green space might be more effective in mitigating emissions of particulate matter [44]. The disparity in these findings could be attributed to the varying influence of plants on air pollutant concentrations at different scales of green spaces. Plants dominate in direct pollutant absorption at larger scales, whereas at more minor scales, pollutant aggregation is mainly influenced by modified ventilation. In the case of neighborhood-scale green spaces, the limited number of plants results in weak pollutant absorption over short periods. Therefore, utilizing concentrated green spaces could facilitate broader ventilation corridors, improving overall area ventilation and reducing the aggregation of bioaerosols.

3. Roadside Green Spaces Retreat effectively diminished bioaerosol accumulation on roads without causing substantial increases in adjacent areas. Roadside Green Spaces Full Retreat particularly established extensive ventilation corridors near pollution sources, showcasing significant efficacy in bioaerosol abatement. In the case of major roads with high pedestrian traffic, adopting partial or complete Roadside Green Spaces Full Retreat alongside building setbacks significantly enhanced bioaerosol abatement.

4. Road Spaces Expansion enhanced ventilation on major roads and significantly reduced local and regional bioaerosol concentrations. This aligns with previous studies on the effects of plants in road canyons, where trees hinder street ventilation, leading to pollutant accumulation [37,38]. Therefore, on congested roads, appropriately narrowing green spaces on both sides improves ventilation, achieving superior bioaerosol abatement while ensuring basic greenery. Additionally, when adjusting green space scales, attention must be paid to the impact of newly added green spaces on surrounding ventilation to prevent the gathering of bioaerosols.

5. Intersection Green Spaces Chamfering proved to be effective in reducing bioaerosol concentrations. Quadrilateral Chamfering, which involves expanding intersection spaces judiciously, demonstrated superior outcomes. However, the effectiveness of Diagonal Chamfering was not solely dependent on its size; Diagonal Double Chamfering showed insignificant changes in bioaerosol concentrations at intersection locations but significantly reduced bioaerosols around intersecting roads. Excessive chamfering may increase wind

speed on upwind roads, causing bioaerosols to accumulate near downwind buildings. This observation aligns with prior studies on pollutant dispersion in street canyons [61]. Utilizing Quadrilateral Chamfering, controlling the chamfering area, and considering green spaces in remaining positions for environmental ventilation offers the most effective strategies for reducing local and general population exposure to bioaerosols.

5. Conclusions

This study utilized ENVI-met software to simulate bioaerosol concentrations within the dormitory area of the Beijing Forestry University campus, exploring the impact of diverse green space ratios and layouts on bioaerosol concentrations in high-density urban areas. The findings illuminate crucial insights. In compact urban environments with limited small-scale green spaces, plant uptake of bioaerosols over brief periods remains constrained. Ventilation conditions emerge as pivotal, significantly influencing bioaerosol concentrations. While introducing more plants, a higher green space ratio could impede ventilation, exacerbating bioaerosol concentration and disease transmission risk. Opting for relatively concentrated green space layouts, even at similar ratios, effectively lowers the site's bioaerosol concentrations to a certain extent. Moreover, strategic interventions such as Roadside Green Spaces Retreat, Road Spaces Expansion, and Intersection Green Spaces Chamfering markedly reduce bioaerosol concentrations in local spots over short durations. These strategies mitigate the risk of substantial bioaerosol exposure during peak commuting hours, positively influencing a local bioaerosol concentration reduction. The results of this study offer insights into the fundamental layout patterns of urban green space construction in the post-pandemic era. Nonetheless, recognizing the variability in population density and microclimates across urban zones, it is imperative to integrate overall and local layouts according to local conditions to diminish bioaerosol concentrations and minimize population exposure to elevated bioaerosol levels.

This study represents a preliminary investigation into the effects of green space ratios and layout patterns on bioaerosol concentrations. In future research, it is advisable to consider combining multiple layout patterns to explore the comprehensive impact of overall green space layouts on bioaerosol concentrations in urban, high-density built-up areas. This would provide specific recommendations for green space layouts while taking into account the current site conditions, allowing for tailored optimal layout solutions. Additionally, due to the significant computational requirements of software simulations, this study exclusively focused on the busiest two hours of pedestrian traffic in early May. However, the actual accumulation of bioaerosol pollutants occurs over extended periods. Future research could extend simulation periods and cover different seasons to investigate the impact of green spaces on bioaerosol concentrations throughout the year, yielding more comprehensive and persuasive results. Furthermore, due to the diverse sources of aerosols in the air and their mixing, the direct measurement of bioaerosol concentrations generated by pedestrian respiration is challenging. In future research, advanced methodologies, including field surveys employing interdisciplinary approaches and specific technical tools to identify and quantify bioaerosols generated by pedestrians, alongside simulation models, could provide empirical validation. This would offer a comprehensive theoretical foundation for post-epidemic urban green space construction.

Author Contributions: Conceptualization, W.J., B.W. and H.H.; methodology, W.J. and H.H.; software, W.J.; validation, W.J. and B.W.; formal analysis, W.J. and H.H.; investigation, W.J. and H.H.; resources, Z.L.; data curation, W.J.; writing—original draft preparation, W.J.; writing—review and editing, W.J.; visualization, W.J. and H.H.; supervision, B.W. and Z.L.; project administration, Z.L. and B.W.; funding acquisition, Z.L. All authors have read and agreed to the published version of the manuscript.

Funding: This research was funded by the National Major Science and Technology Projects of China, grant number 2018ZX07101005.

Institutional Review Board Statement: Not applicable.

Informed Consent Statement: Not applicable.

Data Availability Statement: The data presented in this study are available on request from the corresponding author.

Acknowledgments: The authors wish to convey their appreciation for the hardware facilities and venue support provided by Beijing Forestry University. Furthermore, they extend their sincere gratitude to the editors and reviewers for their invaluable comments and suggestions, which have substantially enhanced the quality of the manuscript.

Conflicts of Interest: The authors declare no conflicts of interest.

Nomenclature

r	radius of bioaerosol droplets, 2.5×10^{-6} m;
ρ	density of bioaerosol droplets, 1×10^{15} $\mu\text{g}/\text{m}^3$;
m	mass of a single biological bioaerosol droplet, μg ;
n	the number of bioaerosol droplets produced by a single cough, 1×10^6 ;
k	ratio of bioaerosol droplets produced by breathing to coughing, 1/10;
M	mass of bioaerosol produced in a single breath, μg ;
v	walking speed of an adult, 1.5 m/s;
t	duration of a single adult breath, 3 s;
l	distance covered by an adult during a single breath, m;
V_0	bioaerosol pollution release rate from an adult, $\mu\text{g}/\text{m}\cdot\text{s}\cdot\text{person}$;
N	pedestrian flow on the road, person/min (Table 1);
V	release rate of the linear pollution source, $\mu\text{g}/\text{m}\cdot\text{s}$;

References

- Brandl, H. Bioaerosols in Indoor Environment—A Review with Special Reference to Residential and Occupational Locations. *Open Environ. Biol. Monit. J.* **2011**, *4*, 83–96. [[CrossRef](#)]
- Ariya, P.A.; Amyot, M. New Directions: The Role of Bioaerosols in Atmospheric Chemistry and Physics. *Atmos. Environ.* **2004**, *38*, 1231–1232. [[CrossRef](#)]
- Archer, J.; McCarthy, L.P.; Symons, H.E.; Watson, N.A.; Orton, C.M.; Browne, W.J.; Harrison, J.; Moseley, B.; Philip, K.E.J.; Calder, J.D.; et al. Comparing Aerosol Number and Mass Exhalation Rates from Children and Adults during Breathing, Speaking and Singing. *Interface Focus* **2022**, *12*, 20210078. [[CrossRef](#)] [[PubMed](#)]
- Yan, J.; Grantham, M.; Pantelic, J.; Bueno De Mesquita, P.J.; Albert, B.; Liu, F.; Ehrman, S.; Milton, D.K.; EMIT Consortium; Adamson, W.; et al. Infectious Virus in Exhaled Breath of Symptomatic Seasonal Influenza Cases from a College Community. *Proc. Natl. Acad. Sci. USA* **2018**, *115*, 1081–1086. [[CrossRef](#)] [[PubMed](#)]
- Van Doremalen, N.; Bushmaker, T.; Morris, D.H.; Holbrook, M.G.; Gamble, A.; Williamson, B.N.; Tamin, A.; Harcourt, J.L.; Thornburg, N.J.; Gerber, S.I.; et al. Aerosol and Surface Stability of SARS-CoV-2 as Compared with SARS-CoV-1. *N. Engl. J. Med.* **2020**, *382*, 1564–1567. [[CrossRef](#)] [[PubMed](#)]
- Acuto, M. COVID-19: Lessons for an Urban(Izing) World. *One Earth* **2020**, *2*, 317–319. [[CrossRef](#)] [[PubMed](#)]
- Bolashikov, Z.D.; Melikov, A.K. Methods for Air Cleaning and Protection of Building Occupants from Airborne Pathogens. *Build. Environ.* **2009**, *44*, 1378–1385. [[CrossRef](#)] [[PubMed](#)]
- Zhen, Q.; Fang, Z.G.; Wang, Y.Q.; Ouyang, Z.Y. Bacterial characteristics in atmospheric haze and potential impacts on human health. *Acta Ecol. Sin.* **2019**, *39*, 2244–2254. [[CrossRef](#)]
- Hu, W.X.; Ding, F.; Song, W.H.; Liu, X.H. The Influence of Green Space Disposition Mode on Bacteria Content in Air. *J. Environ. Health* **2009**, *26*, 546. [[CrossRef](#)]
- Rendana, M. Impact of the Wind Conditions on COVID-19 Pandemic: A New Insight for Direction of the Spread of the Virus. *Urban Clim.* **2020**, *34*, 100680. [[CrossRef](#)]
- Coccia, M. How Do Low Wind Speeds and High Levels of Air Pollution Support the Spread of COVID-19? *Atmospheric Pollut. Res.* **2021**, *12*, 437–445. [[CrossRef](#)] [[PubMed](#)]
- Meo, S.A.; Almutairi, F.J.; Abukhalaf, A.A.; Usmani, A.M. Effect of Green Space Environment on Air Pollutants PM_{2.5}, PM₁₀, CO, O₃, and Incidence and Mortality of SARS-CoV-2 in Highly Green and Less-Green Countries. *Int. J. Environ. Res. Public Health* **2021**, *18*, 13151. [[CrossRef](#)] [[PubMed](#)]
- Wu, X.; Nethery, R.C.; Sabath, M.B.; Braun, D.; Dominici, F. Air pollution and COVID-19 mortality in the United States: Strengths and limitations of an ecological regression analysis. *Sci. Adv.* **2020**, *6*, eabd4049. [[CrossRef](#)]
- Bouketta, S.; Bouchahm, Y. Numerical Evaluation of Urban Geometry's Control of Wind Movements in Outdoor Spaces during Winter Period. *Case Mediterr. Climate. Renew. Energy* **2020**, *146*, 1062–1069. [[CrossRef](#)]
- Leng, J.; Wang, Q.; Liu, K. Sustainable Design of Courtyard Environment: From the Perspectives of Airborne Diseases Control and Human Health. *Sustain. Cities Soc.* **2020**, *62*, 102405. [[CrossRef](#)] [[PubMed](#)]

16. El Samaty, H.S.; Waseef, A.A.E.; Badawy, N.M. The Effects of City Morphology on Airborne Transmission of COVID-19. Case Study: Port Said City, Egypt. *Urban Clim.* **2023**, *50*, 101577. [[CrossRef](#)] [[PubMed](#)]
17. Zhang, J.; Yu, Z.; Zhao, B.; Sun, R.; Vejre, H. Links between Green Space and Public Health: A Bibliometric Review of Global Research Trends and Future Prospects from 1901 to 2019. *Environ. Res. Lett.* **2020**, *15*, 063001. [[CrossRef](#)]
18. Jabbar, M.; Yusoff, M.M.; Shafie, A. Assessing the Role of Urban Green Spaces for Human Well-Being: A Systematic Review. *GeoJournal* **2022**, *87*, 4405–4423. [[CrossRef](#)] [[PubMed](#)]
19. Yli-Pelkonen, V.; Setälä, H.; Viippola, V. Urban Forests near Roads Do Not Reduce Gaseous Air Pollutant Concentrations but Have an Impact on Particles Levels. *Landsc. Urban Plan.* **2017**, *158*, 39–47. [[CrossRef](#)]
20. Oksanen, E.; Kontunen-Soppela, S. Plants Have Different Strategies to Defend against Air Pollutants. *Curr. Opin. Environ. Sci. Health* **2021**, *19*, 100222. [[CrossRef](#)]
21. Lei, Y.; Davies, G.M.; Jin, H.; Tian, G.; Kim, G. Scale-Dependent Effects of Urban Greenspace on Particulate Matter Air Pollution. *Urban For. Urban Green.* **2021**, *61*, 127089. [[CrossRef](#)]
22. Diener, A.; Mudu, P. How Can Vegetation Protect Us from Air Pollution? A Critical Review on Green Spaces' Mitigation Abilities for Air-Borne Particles from a Public Health Perspective—With Implications for Urban Planning. *Sci. Total Environ.* **2021**, *796*, 148605. [[CrossRef](#)] [[PubMed](#)]
23. Huang, Z.; Wu, C.; Teng, M.; Lin, Y. Impacts of Tree Canopy Cover on Microclimate and Human Thermal Comfort in a Shallow Street Canyon in Wuhan, China. *Atmosphere* **2020**, *11*, 588. [[CrossRef](#)]
24. Guo, Y.; Xiao, Q.; Ling, C.; Teng, M.; Wang, P.; Xiao, Z.; Wu, C. The Right Tree for the Right Street Canyons: An Approach of Tree Species Selection for Mitigating Air Pollution. *Build. Environ.* **2023**, *245*, 110886. [[CrossRef](#)]
25. Xing, Y.; Brimblecombe, P. Trees and Parks as “the Lungs of Cities”. *Urban For. Urban Green.* **2020**, *48*, 126552. [[CrossRef](#)]
26. Corada, K.; Woodward, H.; Alaraj, H.; Collins, C.M.; De Nazelle, A. A Systematic Review of the Leaf Traits Considered to Contribute to Removal of Airborne Particulate Matter Pollution in Urban Areas. *Environ. Pollut.* **2021**, *269*, 116104. [[CrossRef](#)] [[PubMed](#)]
27. Ortolani, C. The Importance of Local Scale for Assessing, Monitoring and Predicting of Air Quality in Urban Areas. *Sustain. Cities Soc.* **2016**, *26*, 150–160. [[CrossRef](#)]
28. Huang, C.-W.; Lin, M.-Y.; Khlystov, A.; Katul, G. The Effects of Leaf Area Density Variation on the Particle Collection Efficiency in the Size Range of Ultrafine Particles (UFP). *Environ. Sci. Technol.* **2013**, *47*, 11607–11615. [[CrossRef](#)]
29. Wróblewska, K.; Jeong, B.R. Effectiveness of Plants and Green Infrastructure Utilization in Ambient Particulate Matter Removal. *Environ. Sci. Eur.* **2021**, *33*, 110. [[CrossRef](#)]
30. Shi, Y.; Ren, C.; Lau, K.K.-L.; Ng, E. Investigating the Influence of Urban Land Use and Landscape Pattern on PM_{2.5} Spatial Variation Using Mobile Monitoring and WUDAPT. *Landsc. Urban Plan.* **2019**, *189*, 15–26. [[CrossRef](#)]
31. Taleghani, M.; Clark, A.; Swan, W.; Mohegh, A. Air pollution in a microclimate; the impact of different green barriers on the dispersion. *Sci. Total Environ.* **2020**, *711*, 134649. [[CrossRef](#)] [[PubMed](#)]
32. Dai, F.; Deng, Y.; Chen, M.; Guo, X.H. Effects of Green Space Layout on PM_{2.5} in Different Types of Residential Areas Based on ENVI-met Simulation. *Landsc. Archit.* **2021**, *28*, 70–76. [[CrossRef](#)]
33. Huang, Y.; Lei, C.; Liu, C.-H.; Perez, P.; Forehead, H.; Kong, S.; Zhou, J.L. A Review of Strategies for Mitigating Roadside Air Pollution in Urban Street Canyons. *Environ. Pollut.* **2021**, *280*, 116971. [[CrossRef](#)] [[PubMed](#)]
34. Jin, X.; Yang, L.; Du, X.; Yang, Y. Transport Characteristics of PM_{2.5} inside Urban Street Canyons: The Effects of Trees and Vehicles. *Build. Simul.* **2017**, *10*, 337–350. [[CrossRef](#)]
35. Xue, F. The Impact of Roadside Trees on Traffic Released PM₁₀ in Urban Street Canyon: Aerodynamic and Deposition Effects. *Sustain. Cities Soc.* **2017**, *30*, 195–204. [[CrossRef](#)]
36. Tomson, M.; Kumar, P.; Barwise, Y.; Perez, P.; Forehead, H.; French, K.; Morawska, L.; Watts, J.F. Green Infrastructure for Air Quality Improvement in Street Canyons. *Environ. Int.* **2021**, *146*, 106288. [[CrossRef](#)] [[PubMed](#)]
37. Jeanjean, A.P.R.; Buccolieri, R.; Eddy, J.; Monks, P.S.; Leigh, R.J. Air quality affected by trees in real street canyons: The case of Marylebone neighbourhood in central London. *Urban For. Urban Green.* **2017**, *22*, 41–53. [[CrossRef](#)]
38. Chen, M.; Dai, F.; Yang, B.; Zhu, S. Effects of Urban Green Space Morphological Pattern on Variation of PM_{2.5} Concentration in the Neighborhoods of Five Chinese Megacities. *Build. Environ.* **2019**, *158*, 1–15. [[CrossRef](#)]
39. Li, K.; Li, C.; Liu, M.; Hu, Y.; Wang, H.; Wu, W. Multiscale Analysis of the Effects of Urban Green Infrastructure Landscape Patterns on PM_{2.5} Concentrations in an Area of Rapid Urbanization. *J. Clean. Prod.* **2021**, *325*, 129324. [[CrossRef](#)]
40. Cai, L.; Zhuang, M.; Ren, Y. A landscape scale study in Southeast China investigating the effects of varied green space types on atmospheric PM_{2.5} in mid-winter. *Urban For. Urban Green.* **2020**, *49*, 126607. [[CrossRef](#)]
41. Wu, H.; Yang, C.; Chen, J.; Yang, S.; Lu, T.; Lin, X. Effects of Green Space Landscape Patterns on Particulate Matter in Zhejiang Province, China. *Atmos. Pollut. Res.* **2018**, *9*, 923–933. [[CrossRef](#)]
42. Bi, S.; Dai, F.; Chen, M.; Xu, S. A new framework for analysis of the morphological spatial patterns of urban green space to reduce PM_{2.5} pollution: A case study in Wuhan, China. *Sustain. Cities Soc.* **2022**, *82*, 103900. [[CrossRef](#)]
43. Wu, J.; Xie, W.; Li, W.; Li, J. Effects of Urban Landscape Pattern on PM_{2.5} Pollution—A Beijing Case Study. *PLoS ONE* **2015**, *10*, e0142449. [[CrossRef](#)] [[PubMed](#)]
44. Zhao, S.; Guo, Q.; Gao, N. Influence of Different Vertical Greening Modes on Bioaerosol Control: A Case Study of Environment Simulation of Liujiaping Future Community in Linhai City, Zhejiang Province. *Landsc. Archit.* **2023**, *30*, 94–101. [[CrossRef](#)]

45. Bruse, M. ENVI-Met Implementation of the Gas/Particle Dispersion and Deposition Model PDDM. Available online: <https://www.envi-met.net/documents/sources.PDF> (accessed on 12 June 2023).
46. Salata, F.; Golasi, I.; De Lieto Vollaro, R.; De Lieto Vollaro, A. Urban microclimate and outdoor thermal comfort. A proper procedure to fit ENVI-met simulation outputs to experimental data. *Sustain. Cities Soc.* **2016**, *26*, 318–343. [[CrossRef](#)]
47. Nasrollahi, N.; Hatami, M.; Khastar, S.R.; Taleghani, M. Numerical evaluation of thermal comfort in traditional courtyards to develop new microclimate design in a hot and dry climate. *Sustain. Cities Soc.* **2017**, *35*, 449–467. [[CrossRef](#)]
48. Deshmukh, P.; Isakov, V.; Venkatram, A.; Yang, B.; Zhang, K.M.; Logan, R.; Baldauf, R. The effects of roadside vegetation characteristics on local, near-road air quality. *Air Qual. Atmos. Health* **2019**, *12*, 259–270. [[CrossRef](#)] [[PubMed](#)]
49. Morakinyo, T.E.; Lai, A.; Lau, K.K.-L.; Ng, E. Thermal benefits of vertical greening in a high-density city: Case study of Hong Kong. *Urban For. Urban Green.* **2019**, *37*, 42–55. [[CrossRef](#)]
50. Ma, X.; Zhao, J.; Zhang, L.; Wang, M.; Cheng, Z. The Deviation Between the Field Measurement and ENVI-Met Outputs in Winter-A Cases Study in a Traditional Dwelling Settlement of Northern China. *Environ. Model Assess.* **2023**, *28*, 817–830. [[CrossRef](#)]
51. Gu, K.; Qian, Z.; Fang, Y.H.; Sun, Z.; Wen, H. Influence of vegetation arrangement on PM_{2.5} in urban roadside based on ENVI-met. *Acta Ecol. Sin.* **2020**, *40*, 4340–4350.
52. Liu, J.; Guo, H.; Zhang, L.; Lu, L. Impact of Urbanization on Vegetation Phenology: A Study in the Beijing-Tianjin-Tangshan Region. *Remote Sens. Technol. Appl.* **2014**, *29*, 286–292.
53. Cox, C.S. Physical Aspects of Bioaerosol Particles. In *Bioaerosols Handbook*; Taylor & Francis: Oxfordshire, UK, 1955; pp. 15–25. [[CrossRef](#)]
54. Papineni, R.S.; Rosenthal, F.S. The Size Distribution of Droplets in the Exhaled Breath of Healthy Human Subjects. *J. Aerosol Med.* **1997**, *10*, 105–116. [[CrossRef](#)] [[PubMed](#)]
55. Xie, X.; Li, Y.; Chwang, A.T.Y.; Ho, P.L.; Seto, W.H. How Far Droplets Can Move in Indoor Environments? Revisiting the Wells Evaporation/Falling Curve. *Indoor Air* **2007**, *17*, 211–225. [[CrossRef](#)] [[PubMed](#)]
56. Kong, F.; Nakagoshi, N. Spatial-Temporal Gradient Analysis of Urban Green Spaces in Jinan, China. *Landsc. Urban Plan.* **2006**, *78*, 147–164. [[CrossRef](#)]
57. Yu, Z.; Yang, G.; Zuo, S.; Jørgensen, G.; Koga, M.; Vejre, H. Critical Review on the Cooling Effect of Urban Blue-Green Space: A Threshold-Size Perspective. *Urban For. Urban Green.* **2020**, *49*, 126630. [[CrossRef](#)]
58. Ferrini, F.; Fini, A.; Mori, J.; Gori, A. Role of Vegetation as a Mitigating Factor in the Urban Context. *Sustainability* **2020**, *12*, 4247. [[CrossRef](#)]
59. Nieuwenhuijsen, M.J. New Urban Models for More Sustainable, Liveable and Healthier Cities Post Covid19; Reducing Air Pollution, Noise and Heat Island Effects and Increasing Green Space and Physical Activity. *Environ. Int.* **2021**, *157*, 106850. [[CrossRef](#)] [[PubMed](#)]
60. Elmqvist, T.; Setälä, H.; Handel, S.; Van Der Ploeg, S.; Aronson, J.; Blignaut, J.; Gómez-Baggethun, E.; Nowak, D.; Kronenberg, J.; De Groot, R. Benefits of Restoring Ecosystem Services in Urban Areas. *Curr. Opin. Environ. Sustain.* **2015**, *14*, 101–108. [[CrossRef](#)]
61. Tian, F.; Yu, Z.; Cai, M. Numerical Simulation of Gaseous Pollutants Dispersion at Street-Canyon Road Intersection. *Res. Environ. Sci.* **2008**, *2*, 2180–2183. [[CrossRef](#)]

Disclaimer/Publisher’s Note: The statements, opinions and data contained in all publications are solely those of the individual author(s) and contributor(s) and not of MDPI and/or the editor(s). MDPI and/or the editor(s) disclaim responsibility for any injury to people or property resulting from any ideas, methods, instructions or products referred to in the content.